29th Congress of the International Council
of the Aeronautical Sciences
St. Petersburg, Russia; September 7–12, 2014

FRAMEWORK FOR LOW-NOISE WIND TURBINE BLADE DESIGN

Simão S. Rodrigues, André C. Marta
LAETA, CCTAE, Instituto Superior Técnico, Universidade de Lisboa, Lisboa, Portugal

Abstract

Power production from wind energy has been increasing over the past decades, with more areas being used as wind farms and larger wind turbines (WTs) being built. As the awareness of the impact of wind energy on the environment and human health as also increased, so has the interest in developing fast turnaround WT blade design frameworks capable of predicting both aerodynamic and aeroacoustic performance. In this paper, the development of such framework is described and the results of single and multi operating point optimizations of the blades of the commercial AOC 15/50 WT are presented and discussed. Noise reductions of up to 9.8% were achieved, with a cost of only 1% in energy production.

1 Introduction

For the past few decades, wind energy has seen a significant development, with larger wind turbines (WT) being used and more wind farms being constructed. This led to an increase in awareness of the impacts of wind energy in the environment and human health [1,2,3]. Limitations to generated noise make it necessary to address the issue early in the design phase of the wind turbines. The main objective of this work was to develop a fast turnaround WT blade design framework that could handle noise criteria constraints dictated by specific customer or site location.

2 Prediction Models

To compute the aerodynamic performance of the wind turbine, the Blade Element Momentum (BEM) theory was used, with corrections for the hub- and tip-losses and turbulent wake state. The airfoil 2D data was obtained using the XFOIL [4] viscous-inviscid interactive code. Corrections for 3D effects are applied to the 2D data using a stall delay model [5] and drag adjustments [6]. The corrected data is latter extrapolated using the Viterna method [7]. The Annual Energy Production (AEP) of the wind turbine is computed as

$$AEP = \sum_{i=1}^{N-1} \quad \frac{1}{2}\left(P\left(V_{i+1}\right) + P\left(V_i\right)\right) \\ \times f\left(V_i < V_0 < V_{i+1}\right) \quad \times 8760 \quad , \tag{1}$$

where $P(V_i)$ is the power produced by the wind turbine at a wind speed V_i, $f(V_i < V_0 < V_{i+1})$ is the probability of the wind speed lying between V_i and V_{i+1}, and the constant term refers to the number of hours in a year. The probability density function of the wind is represented by a Weibull distribution.

The aeroacoustic prediction model developed in this work predicts both the turbulent inflow noise and the five mechanisms of airfoil self-noise. Airfoil self-noise is predicted using semi-empirical models developed by Brooks, Pope and Marcolini [8]. Turbulent inflow noise is predicted using a model developed by Amiet [9] and modified my Lowson [10], with corrections to account for the airfoil shape [11,12]. Total noise levels generated by the wind turbine at each frequency level *j* of the 1/3 octave band spectrum are obtained as a sum of the individual contributions of each element,

$$L_{p,j} = 10\log_{10}\left(\frac{N_B}{N_{az}}\sum_i 10^{\frac{L_{p,i}}{10}}\right),$$

$$\tag{2}$$

where N_{az} is the number of azimuthal positions considered for noise prediction and N_B is the number of blades. The Overall Sound Pressure Level (OASPL) can be obtained by summing the noise levels at every frequency,

$$OASPL = 10\log_{10}\left(\sum_j 10^{\frac{L_{p,j}}{10}}\right). \tag{3}$$

3 Implementation

In this section the implementation of both the aeroacoustic prediction tool and Multidisciplinary Design Optimization (MDO) framework is described.

3.1 WT Aeroacoustic Prediction Tool

The aerodynamic and aeroacoustic models were implemented using C++ and Python programming languages. The modules in the different languages were interfaced using SWIG [13]. The tool is robust and flexible, allowing the configuration of the simulations in detail. A representation of the structure of the tool is presented in Fig. 1. The geometry module (represented in the figure by ROTOR and BLADE) represents the WT rotor and its blades, taking as input values of chord, twist, cross-sectional shapes at specific locations of the blade, blade inner an outer radius, hub height and number of blades. This module is called by the ANALYSIS module, when any of these values is required by either the aerodynamic or aeroacoustic models. The analysis itself starts with computing polars of airfoils at certain blade locations (the number and position of the locations is defined by the user). The user can also chose between XFOIL or RFOIL for the computation of the polars (and boundary layer parameters). With the polars computed, the BEM code is run, receiving as input chord and twist values at discretized points of the blade and the computed polars. It outputs spanwise distributions of parameters such as Reynolds number, loading, local angle-of-attack, local velocity, etc, as well as the produced AEP. The

NOISE module is then called, receiving as input the spanwise distributions of parameters like angle-of attack, velocity and Reynolds number (amongst others) and the boundary layer parameters are computed for each of the discretized element (the computational surface nodes for the aerodynamic and aeroacoustic analyses are independent of each other). With these boundary layer parameters, the noise for each element is computed and summed as indicated in Eqs. (2) and (3), outputting the OASPL value for that WT rotor.
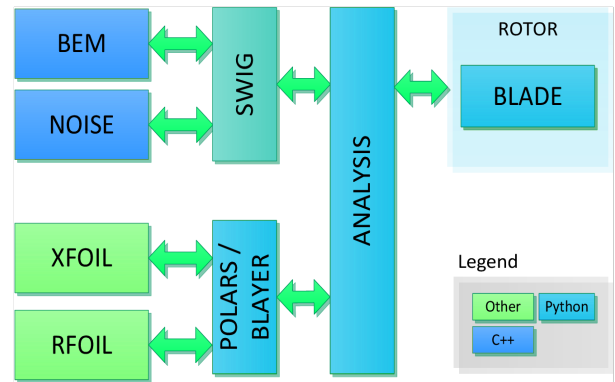

Fig. 1. Structure of the WT aeroacoustic prediction tool.

3.2 Shape Parametrization

The shape of the blade was parametrized by a set of control points defining the twist and chord distributions, which were either linearly interpolated or used to construct Bézier curves, and a set of control airfoil sections. After a survey of the most commonly used methods in airfoil shape parametrization, an approach was chosen using Non-Uniform Rational Basis Splines (NURBS) curves for the upper and lower curves of the airfoil. The main advantages of using NURBS include the direct connection between parameters and geometry, easy controllability of inflection points and local approximation [14]. Each curve is defined by seven control points and a knot vector (see Fig. 2), totaling 20 degrees of freedom for the total airfoil. Points 0 and 12, located at the airfoil trailing edge, can only move vertically to guarantee unitary chord profiles. This parametrization was demonstrated to be able to accurately represent various WT airfoil geometries.
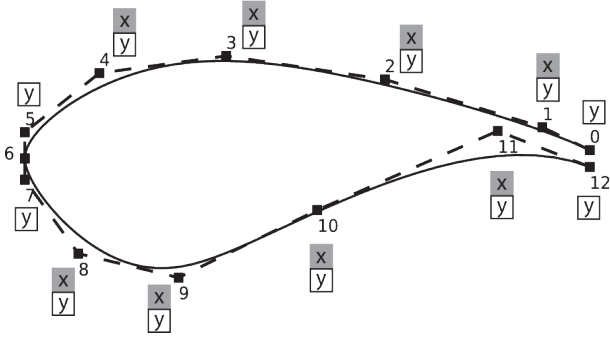
29th Congress of the International Council
of the Aeronautical Sciences
St. Petersburg, Russia; September 7–12, 2014

Fig. 2. NURBS airfoil parametrization control points and respective degrees of freedom

Fig. 3. Flowchart of the optimization framework

3.3 Optimization Framework

A Multi-Disciplinary Optimization (MDO) framework was developed using the Python optimization module pyOpt [15] and the previously described prediction tool and geometry parametrization modules. The Non-dominated Sorting Genetic Algorithm (NSGA-II) [16] was chosen as the optimization algorithm due to its multi-objective capability and proven use in the optimization of wind turbines. In the optimization cases presented in this paper, the parameters used are for the probability of occurrence of crossover and mutation and the distribution indexes for the same two operations are presented in Tab. 1.

Parameter	Value
P(crossover)	0.6
P(Mutation)	0.2
η_c	10.0
η_m	20.0
Seed	0.0

Tab.1. Genetic algorithm parameters used in the optimizations.

Each optimization is set up by a python script, where the objective functions and optimization parameters (such as the ones presented in Tab. 1, as well as the design variables) are defined. All these parameters are input to pyOpt, which acts as an interface to the actual optimizer. A flowchart of the optimization framework is shown in Fig. 3.
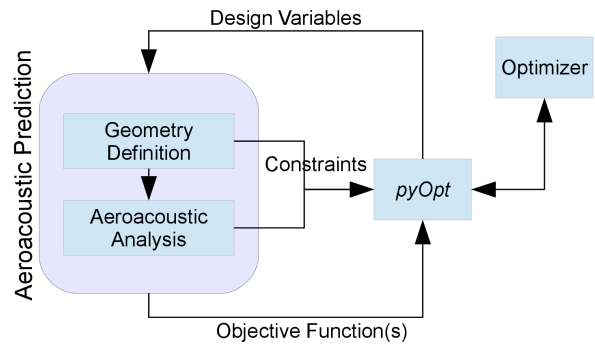
3.4 Validation of the aeroacoustic prediction code

The prediction tool was validated against experimental data obtained from the commercial AOC 15/150 50 kW wind turbine [17]. Both the aerodynamic and aeroacoustic predictions can be said to provide qualitative results sufficient for the conceptual design framework that it is intended for [18].

4 Results

The results of two optimization cases performed on the AOC 15/50 WT blade are presented in this section. The turbine has a rated power of 50 kW and each one of its three blades has a length of 7.5 m. It uses the NREL S821, S819 and S820 profiles, defined ad 40, 75 and 95 % of the blade pan, respectively. The multi-objective optimization problems aimed the maximization of the AEP while minimizing the OASPL produced by the WT. They can be posed in standard form as

$$\begin{aligned} \text{minimize} \quad & f_1(\mathbf{x}) = -AEP \\ \text{and} \quad & f_2(\mathbf{x}) = OASPL \end{aligned}, \quad (4)$$

$$\begin{aligned} \text{subject to} \quad & \mathbf{g}(\mathbf{x}) \leq 0, \\ & \mathbf{x}^L < \mathbf{x} < \mathbf{x}^U, \end{aligned} \quad (5)$$

where $\mathbf{g}$ is a set of 56 constraints that guarantee that the control points do not cross each other and that the new shape maintains an airfoil like shape [18].

For the simulations, a Weibull curve with parameters A = 6.48 m/s and k = 1.99 was

assumed, representing the wind distribution in the Portuguese municipality of Vila do Bispo, in the south west of Portugal.

The BEM calculations were run for wind speeds raging from 4 to 25 m/s, in 1 m/s intervals, and the noise was computed assuming the observer at ground level and 96 m downwind of the turbine, in de direction of its rotation axis. A terrain with many bushes and obstacles was assume, resulting in a selected ground roughness of 0.5 m. Aerodynamic data of the airfoils was computed using XFOIL and the trailing edge thickness of the airfoils assumed to be 1 % of the chord, with a constant angle of 6º. The noise was only computed in the 60% outer part of the blade, due to the non-aerodynamic shape of the cross sections up to 40 % of blade span.

Bézier curves of 5th order were used to define the twist distribution along the blade, resulting in 6 design variables. The chord, defined by linear interpolation of 3 control points (the first being fixed at the hub), contributed with 2 design variables. Four control sections defining the airfoil shapes were used, being the one at the hub considered frozen as a circle. At each section, the coordinates of 10 control points were used as design variables. As the y-coordinates of control points 0 and 12 were kept constant, each control section introduced 18 design variables, resulting in 54 variables. As such, the total number of design variables was 62. The design variables of the control sections were allowed to move ±10% in the x-direction and ±30% in the y-direction, relative to the initial control points, while the chord variables were allowed to take values between y - 0.3 m and y + 0.6 m, where y is the initial chord value Twist was allowed to vary from -15 to 15º.

The set of constraints used to impose feasible geometries is described in detail in [18].

4.1 Single Operating Point Optimization

The Single Operating Point (SOP) optimization started with a baseline blade producing an AEP of 116.75 MWh and an Overall Sound Pressure Level (OASPL) at 6 m/s of 55.33 dB(A). The optimizer ran for 140 generations of 68 individuals and the resultant solutions are presented in the Pareto front shown in Fig. 4.

Noise reduction of about 5 dB(A) with insignificant reduction in AEP is obtained with the minimum noise solution. The maximum AEP is able to reduce the noise considerably while increasing the AEP value and the trade-off solution, also highlighted in the figure, is able to reduce the noise to levels close to the minimum noise and increase the AEP to levels close to the maximum AEP solution.
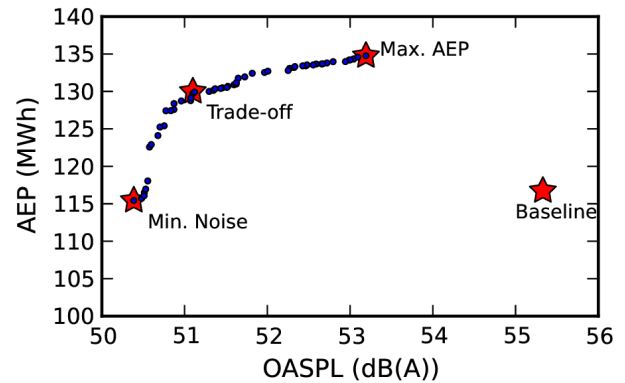

Fig. 4. Pareto front for the SOP optimization

Chord and twist distributions of the three solutions highlighted in Fig. 4 are presented in figures 5 and 6, respectively. The maximum AEP blade presents the highest tapper towards the tip of the blade, which contradicts the expectations, as the noise is mainly generated in the outer part of the blade. This may be explained by the reduced loading of the blade due to the cross-sectional shape of the airfoils in that outer region. In terms of twist, all the optimized blades present higher values near the root, when compared to the baseline, and follow the same trend, with the minimum noise solution always presenting slightly lower values than the other two (mainly near the tip).
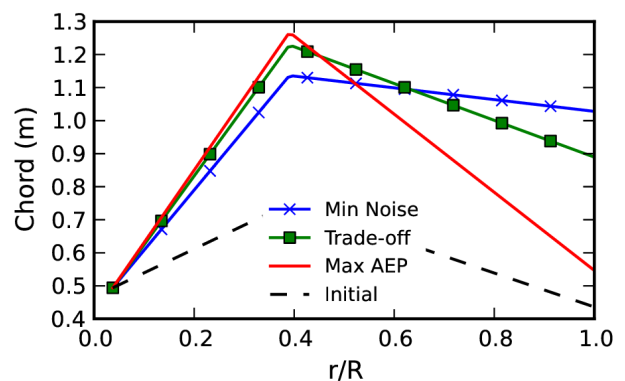

Fig. 5. Chord distributions of optimized blades (SOP optimization)

29th Congress of the International Council
of the Aeronautical Sciences
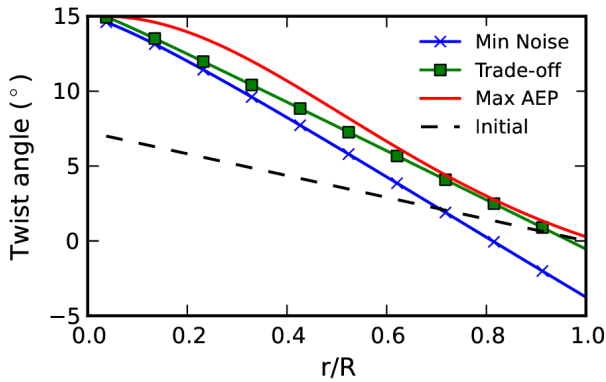St. Petersburg, Russia; September 7–12, 2014

Fig. 6. Twist distributions of optimized blades (SOP optimization)

The baseline and optimized airfoil shapes of the same highlighted solutions are presented in Fig. 7. The maximum AEP and trade-off geometries at 40% of the blade present a slight increase in camber in the front part of the airfoil. The same change is visible at 75% of the blade, while the minimum noise airfoil at this section presents a slight decrease in camber. All three optimized airfoils present lower thickness than the baseline, at this station. At 95% of blade span there is a general increase in camber of the three optimized airfoils, which do not present significant differences between each other.

a) 40 % of blade span

b) 75 % of blade span

c) 95 % of blade span
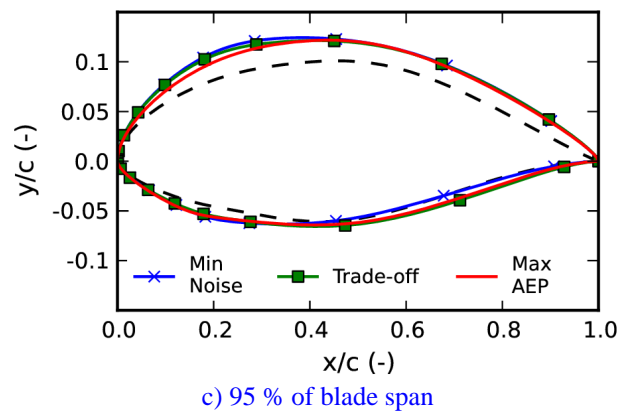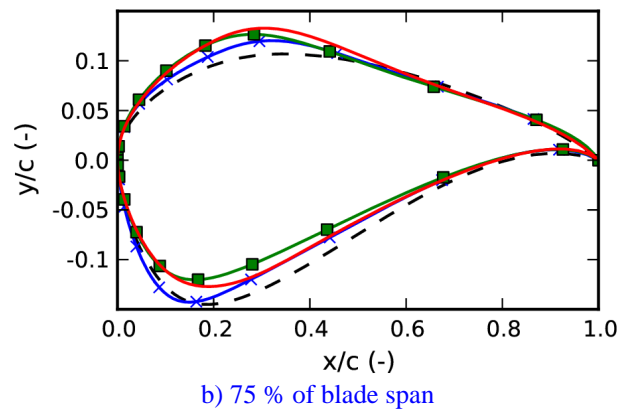
Fig. 7. Initial and optimized airfoil shapes of SOP optimization
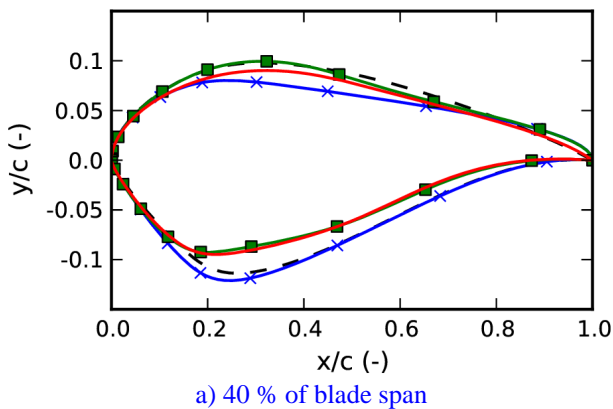
The noise produced by the WT blades in the rotor plane is presented in Fig. 8, where the asymmetry due to the observer not being on the rotor axial axis is visible, with higher OASPL values between 90º and 180º (downward motion of the blade).
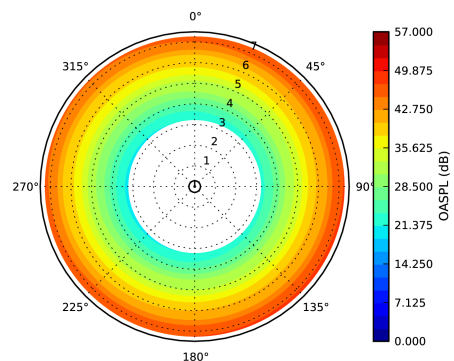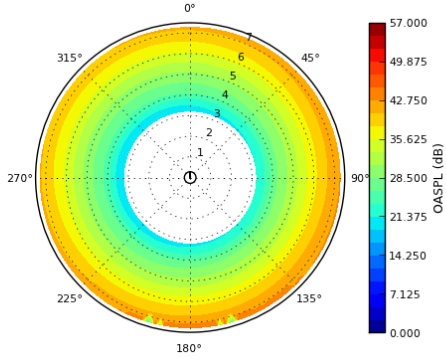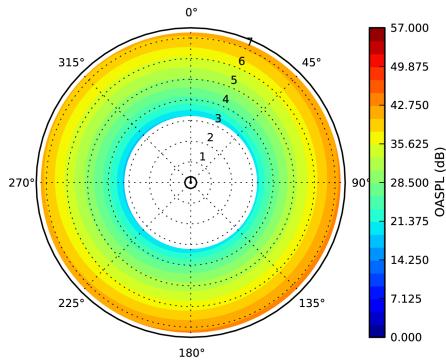

Fig. 8. Sound pressure levels across the rotor with the baseline blades.

A similar representation of the noise on the rotor plane is shown, for the three solutions, in
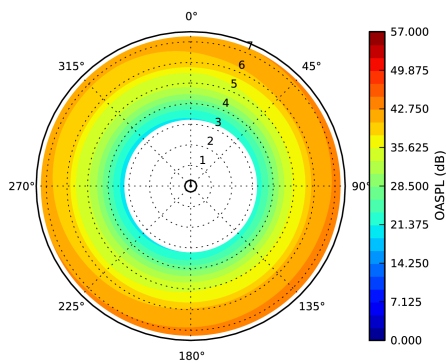
Fig. 9. It is visible the minimum noise and trade-off solutions present much lower noise levels than the baseline. The maximum AEP solution, although presenting slightly higher noise levels around the middle of the blade, produces lower levels elsewhere, particularly in the outer region of the rotor.

a) Minimum noise

b) Trade-off

c) Maximum AEP

Fig. 9. Sound pressure levels across the rotors using the three selected optimized blades of the SOP optimization case.

4.2 Multi Operating Point Optimization

A Multi Operating Point (MOP) optimization was also performed, taking into account the noise generated at two different wind speeds (6 and 8 m/s). This aimed at obtaining blade geometries better fitted for a wider range of operating conditions. The objective function relative to noise was redefined to account for the noise at different wind speeds as

$$f_2 = \frac{10 \log_{10} \sum_{i=1}^{n} h_i 10^{OASPL_i/10}}{\sum_{i=1}^{n} h_i}, \qquad (6)$$

where h_i are weight factors based on the Weibull distribution of the wind. The optimization was run for 70 generations (due to the increased computational cost and time constraints) of 68 generations. The resulting solutions are presented in Fig. 10, where three solutions are highlighted, one corresponding to maximum AEP value, minimum noise production and a trade-off between the other two.
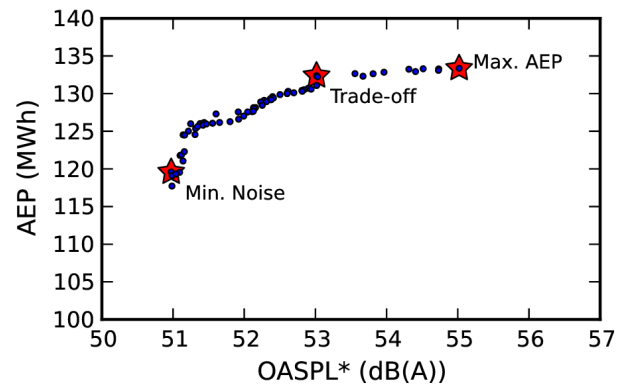

Fig. 10. Pareto front for the MOP optimization

Chord and twist distributions of the solutions highlighted in the previous figure are presented in figures 11 and 12, respectively. As in the SOP case, the maximum AEP solution presents higher tapper than the other two solutions. Regarding the twist distribution, similar distributions as the ones in the SOP are obtained in this MOP optimization.

29th Congress of the International Council
of the Aeronautical Sciences
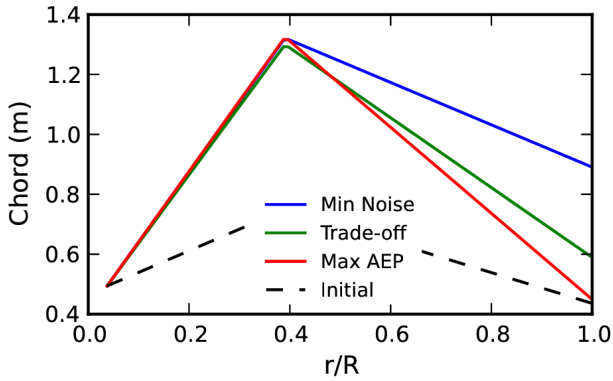St. Petersburg, Russia; September 7–12, 2014

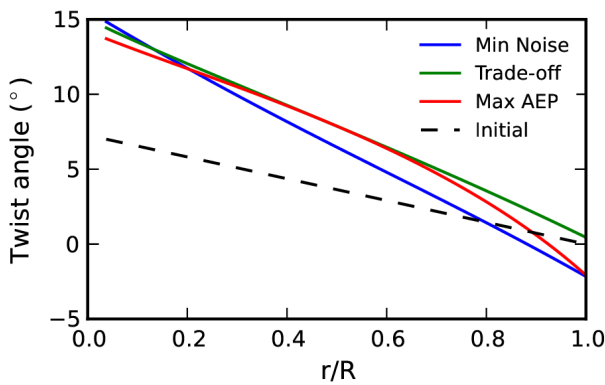Fig. 11. Chord distributions of optimized blades (MOP optimization)

Fig. 12. Twist distributions of optimized blades (MOP optimization)

Figure 13 presents the optimized profiles of the three selected solutions, at the three control sections, located at 40, 75 and 95 % of blade span. A first look at the figure shows that the trade-off geometry is closer to the maximum AEP one near the root (40 % of blade span) and close to the minimum noise geometry at 95 % of blade span, a result of the noise levels being stronger towards the tip of the blade. At 40 % of the blade, there is a reduction of maximum thickness in the maximum AEP and trade-off geometries, while the minimum noise airfoil the maximum thickness is increased. The same can be said about the airfoils at 75 % of blade span, with the exception of the minimum noise airfoil, which does not present a higher thickness to chord ratio than the baseline profile. At 95 % of blade span there is an increase of fore camber and thickness of all three profiles and, for the trade-off and minimum noise solutions, the same is visible in the aft of the airfoil.
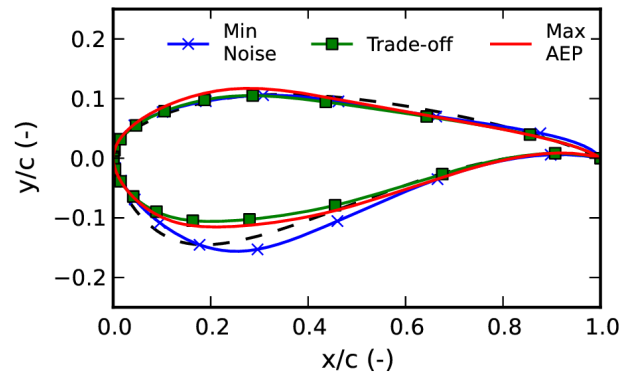

a) 40 % of blade span
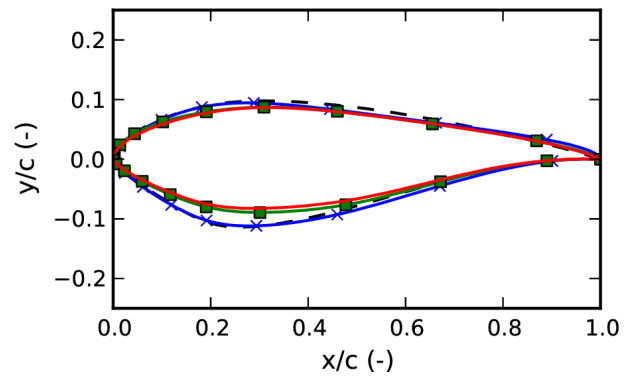
b) 75 % of blade span
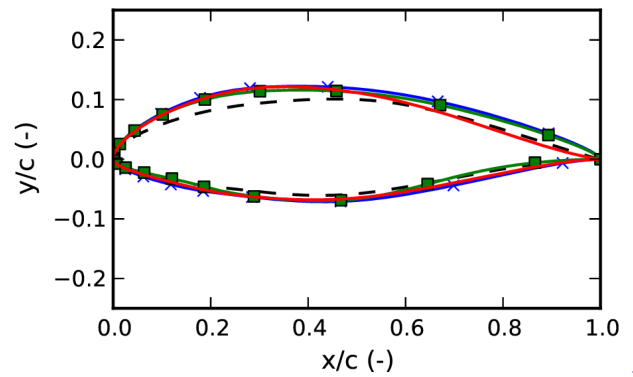
c) 95 % of blade span

Fig. 13 Initial and optimized airfoil shapes of SOP optimization

Similarly to Fig. 9, the sound pressure levels across the rotor plane of the three highlighted solutions of the MOP optimization case are presented in Fig. 14, for wind speed of 6 m/s. In this case, the differences between the three solutions are more clear, particularly between the minimum noise and the trade-off, as they are further apart in the horizontal axis of Fig. 10.
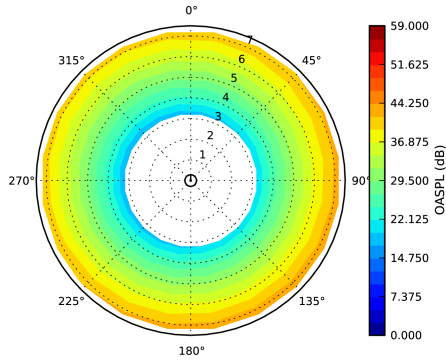
a) Minimum noise
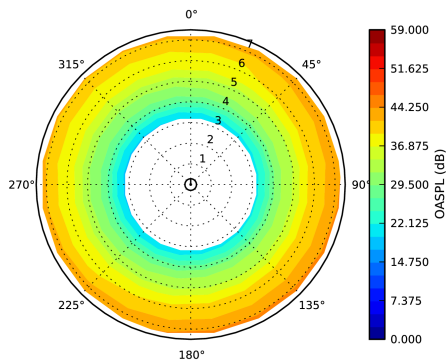
c) Trade-off
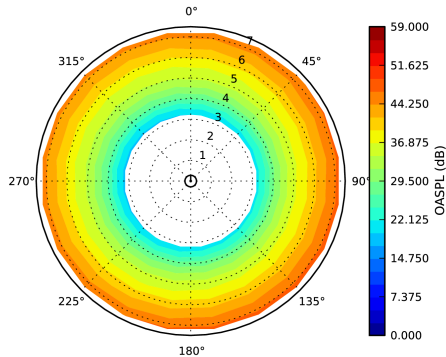
d) Maximum AEP

Fig. 14 Sound pressure levels across the rotors using the three selected optimized blades of the MOP optimization case.

The AEP and OASPL values of the two optimization cases are presented in Tab. 2. The higher OASPL values of the MOP cases are due to these values being calculated with Eq. (3), and thus, taking into account the OASPL at higher wind speeds (8 m/s). The SOP case is able to reduce noise by 9.8 %, at a cost of 1 % in AEP. A reduction of 4 % in noise levels is also achieved, but with an increase in AEP of 15%. In the MOP optimization, the reductions/gains are similar but slightly smaller.

A maximum gain in AEP of 14% is achieved with a reduction of 1% in noise levels, while the maximum noise reduction achieved is of 8%, while still increasing AEP by 2%.

		AEP [MWh]		OASPL[dB(A)]	
	Baseline	116.74		55.33	
SOP	Min Noise	115.45	-1 %	50.38	-9.8 %
	Max AEP	134.76	15 %	53.19	-4 %
	Baseline	116.74		55.39	
MOP	Min Noise	119.58	2 %	50.97	-8 %
	Max AEP	133.36	14 %	55.02	-1 %

Tab. 2. Optimal AEP and OASPL values from SOP and MOP optimization cases

A comparison of the computational time required for the two optimization cases presented in this paper is shown in Fig. 15, where an hypothetical MOP case with 4 operating points is also extrapolated. It is clear that doubling the number of operating cases does not double the computational time, as the aerodynamic analysis is only performed once per function call. From the two optimization cases, the factor by which the computational time of an optimization with n operating points would increase is approximated by $k \approx 0.8n + 0.2$. The SOP case took 23.6 CPU hours to complete, with an average of 8.93 seconds per function call, on a single core of an Intel® Core™ i7-3820 CPU @ 3.60GHz with 64 GB of RAM.
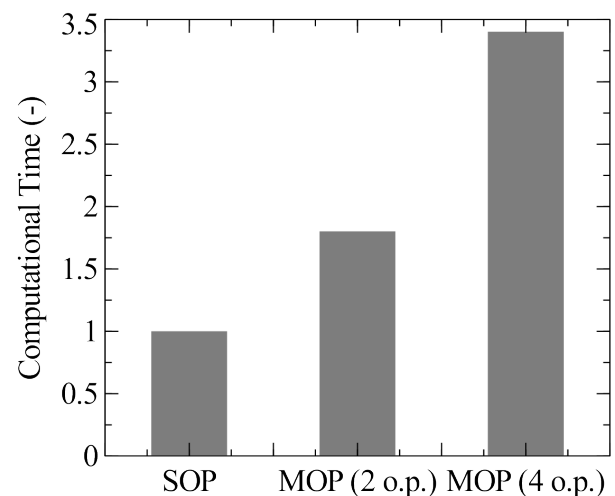

Fig. 15. Comparison of the computational time between SOP and MOP optimization cases

29th Congress of the International Council
of the Aeronautical Sciences
St. Petersburg, Russia; September 7–12, 2014

5 Conclusions

Using the developed framework, it was possible to successfully address noise constraints by fully varying the geometry of the blade of a commercial WT. The NSGA-II algorithm produced Pareto fronts comprising a set of solutions for both single and multi operating point optimization cases. These optimal blade geometries were capable of producing lower noise than the baseline, while maintaining or even increasing energy production. The fact that a set of optimal geometries is obtained, and not only one optimal geometry, allows the designer to chose the one (or ones) that better suits its needs and further improve it from there, thus making it very useful in the early stages of the design of a WT blade. The SOP optimization case took about 23 CPU hours to finish, which can easily be reduced since the genetic algorithm is inherently parallelizable. In a simple workstation with a 4-core CPU, the same run time could be reduced to about 6 hours, making the conceptual design framework a fast-turnaround tool.

References

[1] Stephen D.G., Sphepherd K., Hubbard H., Grosveld F. (1982). Guide to the evaluation of human exposure to noise from large wind turbines, NASA TM 83288.

[2] Pedersen, E., & Waye, K. P. (2004). Perception and annoyance due to wind turbine noise—a dose–response relationship. *The Journal of the Acoustical Society of America*, 116(6), 3460-3470.

[3] Colby, W. D., Dobie, R., Leventhall, G., Lipscomb, D. M., McCunney, R. J., Seilo, M. T., & Søndergaard, B. (2009). Wind turbine sound and health effects. *An expert panel review: American Wind Energy Association & Canadian Wind Energy Association*.

[4] Drela M. (1989). XFOIL: An analysis and design system for low Reynolds number airfoils, *Low Reynolds numbers aerodynamics*.

[5] Du, Z., & Selig, M. S. (1998). A 3-D stall-delay model for horizontal axis wind turbine performance prediction. In *Proceedings of the 1998 ASME wind energy symposium, Reno, NV* (pp. 9-19).

[6] Eggers, A. J., Chaney, K., & Digumarthi, R. (2003). An assessment of approximate modeling of aerodynamic loads on the UAE rotor. In *ASME 2003 Wind Energy Symposium* (pp. 283-292). American Society of Mechanical Engineers.

[7] Viterna, L. A., & Janetzke, D. C. (1982). *Theoretical and experimental power from large horizontal-axis wind turbines* (No. DOE/NASA/20320-41; NASA-TM-82944). National Aeronautics and Space Administration, Cleveland, OH (USA). Lewis Research Center.

[8] Brooks T., Pope D., Marcolini M. (1989). Airfoil self-noise and prediction, *National Aeronautics and Space Administration*, Vol. 1218, US.

[9] Amiet R. (1975). Acoustic radiation from an airfoil in a turbulent stream. *Journal of Sound and Vibration*, 41(4):407-420.

[10] Lowson M. (1993). Assessment and prediction of wind turbine noise, *Energy Technology Support Unit*.

[11] Moriarty P., Guidati G., Migliore P. (2004). Recent improvement of semi-empirical aeroacoustic prediction code for wind turbines, *10th AIAA/CEAS Aeroacoustic Conference*, Manchester, UK.

[12] Moriarty P., Guidati G., Migliore P. (2005). Prediction of turbulent inflow and trailing-edge noise for wind turbines, *11th AIAA/CEAS Aeroacoustic Conference (26th Aeroacoustic Conference)*.

[13] Beazley, D. M. (1996). SWIG: An easy to use tool for integrating scripting languages with C and C++. In *Proceedings of the 4th USENIX Tcl/Tk workshop* (pp. 129-139).

[14] Piegl, L. A., & Tiller, W. (1997). *The NURBS book* (2nd ed.). Berlin: Springer.

[15] R. E. Perez, P. W. Jansen, and J. R. R. A. Martins. (2012). pyOpt: A Python-based object-oriented framework for nonlinear constrained optimization. *Struct Multidiscip Optim*, 45(1):101-118 doi:10.1007/s00158-001-0666-3

[16] Deb, K., Pratap, A., Agarwal, S., & Meyarivan, T. A. M. T. (2002). A fast and elitist multiobjective genetic algorithm: NSGA-II. *Evolutionary Computation, IEEE Transactions on*, 6(2), 182-197.

[17] Seaforth Energy (2010) AOC 15/50 Specification Sheet. http://seaforthenergy.com/wp-content/uploads/2010/12/AOC1550-Specification-Sheet.pdf

[18] Rodrigues S., Marta A. (2014). On addressing noise constraints in the design of wind turbine blades, *Struct Multidiscip Optim*, Springer, doi:10.1007/s00158-014-1072-4, In Press.

Contact Author Email Address

Simão S. Rodrigues
Instituto Superior Técnico
Av. Rovisco Pais 1,
1049 Lisboa, Portugal
Email: simao.rodrigues@tecnico.ulisboa.pt
Tel.: +351 218419466

Copyright Statement